Science in China Series E: Technological Sciences

www.scichina.com
tech.scichina.com
www.springerlink.com

Microstructure refinement and magnetic properties enhancement of nanocrystalline $Nd_{12.3}Fe_{81.7}B_{6.0}$ ribbons by addition of Zr

BAO XiaoQian†, QIAO Yi, GAO XueXu, ZHU Jie & ZHOU ShouZeng

State Key Laboratory for Advanced Metals and Materials, University of Science and Technology Beijing, Beijing 100083, China

Effects of Zr addition and annealing treatment on the formation, microstructure and magnetic properties of $Nd_{12.3}Fe_{81.7-x}Zr_xB_{6.0}$ (x=0—3.0) ribbons melt-spun and annealed have been systematically investigated by means of vibrating sample magnetometer (VSM), differential scanning calorimeter (DSC), X-ray diffraction (XRD), and high resolution scanning electron microscopy (HRSEM). Phase analysis reveals that $Nd_2Fe_{14}B$ is single-phase material. It has been found that the intrinsic coercivity H_{ci} of the optimally processed $Nd_{12.3}Fe_{81.7-x}Zr_xB_{6.0}$ ribbons increases monotonically from 751.7 kA/m for x=0 to 1005.3 kA/m for x=3.0. The remanence polarization J_r and maximum energy product $(BH)_{max}$ increase first with Zr addition, then slightly decrease with further increasing Zr content. Optimum magnetic properties with J_r=1.041 T, H_{ci}=887.5 kA/m and $(BH)_{max}$=175.2 kJ/m^3 have been achieved for the ribbons with x=1.5. The significant improvement of magnetic properties originates from the finer grains of the ribbons by introducing Zr.

Nd-Fe-B magnets, nanocrystalline, microstructure, magnetic properties

Since the discovery of the nanocrystalline Nd-Fe-B magnets, extensive efforts have been made to improve magnetic properties of $Nd_2Fe_{14}B$ based magnets[1−3]. It has been shown that isotropic nanocrystalline Nd-Fe-B magnets processed by melt spinning can be divided into three main groups with respect to Nd content: (1) ribbons of low Nd content (3—11 at%) have an great remanence, but the coercive field is too low for most of the major industrial applications[4−6]; (2) ribbons with high Nd content (over 13 at%) have a very high coercivity due to the well-isolated single domain particles by paramagnetic Nd-rich phase, but the remanence is decreased by the presence of Nd-rich phase[7,8]; (3) ribbons of stoichiometric or near-stoichiometric Nd (11—13 at%) alloys show a relatively high coercivity and enhanced remanence due to extensive exchange coupling between the ultra-fine $Nd_2Fe_{14}B$ grains without secondary phase[9], spontanously. In the present investigation, we focus on nanocrystalline Nd-Fe-B alloys with Nd content near 12 at%. Since the magnetic properties of nanocrystalline magnets are highly sensitive to microstructure, extensive efforts have been made to optimize the nano-structure by altering the alloy compositions[10], adding various alloying elements[11,12] and controlling the cooling rates[13] or post annealing conditions[14]. Among various microalloying elements, Zr addition is found to be an effective way to decrease the sizes of crystallized phases, thereby increasing exchange coupling and coercivity[15]. The processing window for producing Nd-Fe-B melt-spun ribbons with optimum magnetic properties by direct quenching to a nanocrystalline structure is narrow. One way to overcome this is to produce amorphous material by overquenching, followed by annealing to obtain the desired microstructure. In this paper, we concentrate our studies on the influence of Zr addition to a near stoichiometric $Nd_{12.3}Fe_{81.7}B_{6.0}$ nanocrystalline alloy by

Received September 22, 2008; accepted November 5, 2008
doi: 10.1007/s11431-009-0131-3
†Corresponding author (email: bxq118@skl.ustb.edu.cn)

melt spinning and subsequent annealing on the magnetic properties and microstructure.

1 Experimental procedure

The alloy ingots with nominal composition of $Nd_{12.3}Fe_{81.7-x}Zr_xB_{6.0}$ (x=0, 0.5, 1.0, 1.5, 2.0, 2.5, 3.0) were prepared by arc melting from Nd, Pr, Fe, Zr, and Fe-B constituents under an Ar atmosphere. The ingots were re-melted four times to ensure homogeneity. After being crushed, small pieces of about 6—8 g each to accommodate the size of the crucible were used for melt spinning under argon. Ribbons with 2—3 mm in width and 30—60 μm in thickness were obtained by ejecting the molten alloys from a quartz tube with an orifice diameter about 0.6 mm onto a copper wheel at surface speeds (V_s) of 22 m/s. These amorphous flakes were then sealed in a quartz tube under the vacuum of 2×10^{-3} Pa and annealed at 823—1023 K for 10 min to crystallize and develop a desired fine nanoscale microstructure and optimize the coercivity. The tube were put into the furnace that had been pre-heated to the desired temperature, hold for the desired time, and then taken out to cool in the water. The thermal analysis of the ribbons was carried out using a NETZSCHSTA449 differential scanning calorimeter at a heating rate of 10 K/min. The phases and the degree of crystallinity of the samples were characterized by D/max-rB X-ray diffractometer (CuKα radiation). Microstructural studies were characterized by high resolution scanning electron microscopy (HRSEM, model ZEISS SUPRA55). The observation were made on the fracture surface through thickness of the ribbons with no further surface preparation. Hysteresis loops of the ribbons were measured using a LDJ 9600 vibrating sample magnetometer with an applied field of up to 1600 kA/m. The length direction of the ribbons was parallel to the applied field in order to minimize demagnetization effect.

2 Results and discussion

2.1 Microstructure and magnetic properties of melt-spun ribbons

Figure 1 shows XRD patterns of the melt-spun $Nd_{12.3}Fe_{81.7-x}Zr_xB_{6.0}$ ribbons with the wheel speed of 22 m/s. It can be seen that the quantity and the relative intensity of

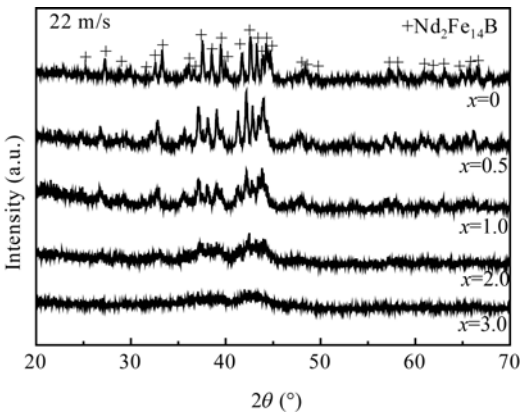

Figure 1 XRD patterns of melt-spun $Nd_{12.3}Fe_{81.7-x}Zr_xB_{6.0}$ ribbons by 22 m/s.

diffraction peak for 2∶14∶1 decreases with increasing Zr content x, suggesting that the amount of 2∶14∶1 phase decreases and amorphous phase increases with increasing Zr content. The ribbons with $x=0$ and $x=0.5$ consist of hard magnetic 2∶14∶1 phase and few amorphous phase. The XRD patterns of the ribbons with x = 1.0 comprise crystalline phases of 2∶14∶1 and small amount of amorphous phase, and those of the ribbons with $x=3.0$ present primarily amorphous phase. This indicates that Zr addition improves significantly the amorphousizing tendency of $Nd_{12.3}Fe_{81.7-x}Zr_xB_{6.0}$ ($x=0$—3.0) alloys.

The typical hysteresis loops of the $Nd_{12.3}Fe_{81.7-x}Zr_xB_{6.0}$ melt-spun ribbons by 22 m/s are shown in Figure 2. It is clear that the permanent magnetic properties of the melt-spun ribbons decrease drastically with increasing Zr content. The demagnetization curve is smooth and shows good squareness for the sample with $x=0.5$ but shows a very low coercivity and the distinct kink for samples with $x\geqslant1.5$. This is in good agreement with XRD analysis in Figure1, since the shapes of hysteresis

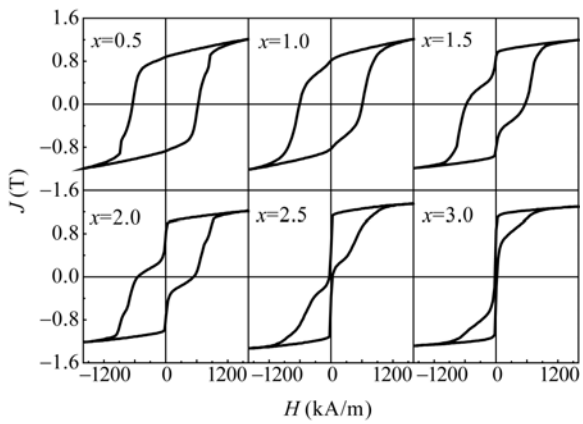

Figure 2 Hysteresis loops of melt-spun $Nd_{12.3}Fe_{81.7-x}Zr_xB_{6.0}$ ribbons by 22 m/s.

loop are very sensitive to microstructure. It also means that the optimal wheel speeds shift to low values with increasing Zr content.

Figure 3 shows the differential scanning calorimetry (DSC) curves of the melt-spun $Nd_{12.3}Fe_{81.7-x}Zr_xB_{6.0}$ ribbons at a heating rate of 10 K/min from room temperature to 1173 K. The ribbon with $x = 0.5$ shows no exothermic peak, further verifying no residual amorphous phase in the melt-spun ribbons. The ribbons with $x = 1.5$ and 2.5 show one exothermic peak corresponding to transformation from amorphous to 2∶14∶1 structure. Compared to the ribbon with $x = 1.5$, the crystallization temperature peak T_p for the ribbon with $x = 2.5$ increases by approximately 30 K, indicating that Zr element enhances the thermal stability of amorphous phase in Nd-Fe-B alloy. Enrichment of Zr atoms along grain boundary stabilizes amorphous phase in the melt-spun and annealing process of the ribbons, which is believed to be a main reason that thermal stability is enhanced by Zr addition in the studied nanocrystalline $Nd_{12.3}Fe_{81.7}B_6$ magnets.

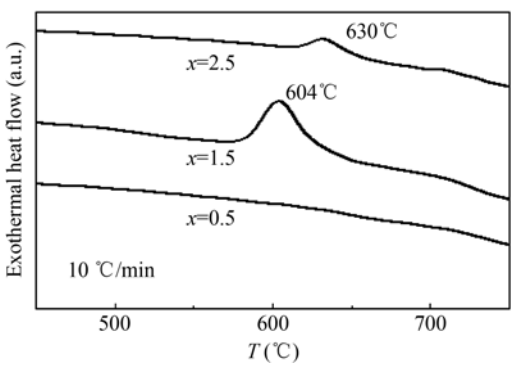

Figure 3 DSC curves for melt-spun $Nd_{12.3}Fe_{81.7-x}Zr_xB_{6.0}$ ribbons.

2.2 Influence of annealing treatment on magnetic properties

The intrinsic coercivity H_{ci}, remanence polarization J_r and maximum energy product $(BH)_{max}$ of the melt-spun ribbons are relatively low, which can be ascribed to incomplete crystallization of the ribbons, as evidenced by the superposition of broad peaks of amorphous precursor alloy and the characteristic of 2∶14∶1 peaks shown in Figure 1. In order to achieve the best magnetic properties for each alloy, a thermal treatment is employed individually to quenched ribbons to induce a fine grain structure crystallizing from the amorphous state. Figure 4 summarizes the effect of annealing temperature T_a on H_{ci}, J_r and $(BH)_{max}$ of $Nd_{12.3}Fe_{81.7-x}Zr_xB_{6.0}$ ribbons. It can be seen that H_{ci}, J_r and $(BH)_{max}$ increase first with increasing T_a until reaching the maximum values, then decrease with further increasing T_a. However, an extraordinarily high remanence ratio of 0.75 is achieved at optimum T_a, which indicates a strong intergranular exchange coupling. The optimum T_a increases with increasing Zr content in the alloys, which is in good agreement with the differential thermal analysis in Figure 3. Optimum magnetic properties with $J_r = 1.041$ T, $H_{ci} = 887.5$ kA/m and $(BH)_{max} = 175.2$ kJ/m^3 are achieved by annealing the melt-spun ribbons with x=1.5 at 898 K for 10 min.

In order to better understand the influence of annealing treatment on magnetic properties of the ribbons, Figures 5 and 6 show the hysteresis loops and XRD patterns of the ribbons with $x = 3.0$ in melt-spun and devitrification annealing states, respectively. The shape of the hysteresis loop of nanophase magnets is highly sensitive to their microstructure. The melt-spun ribbons show

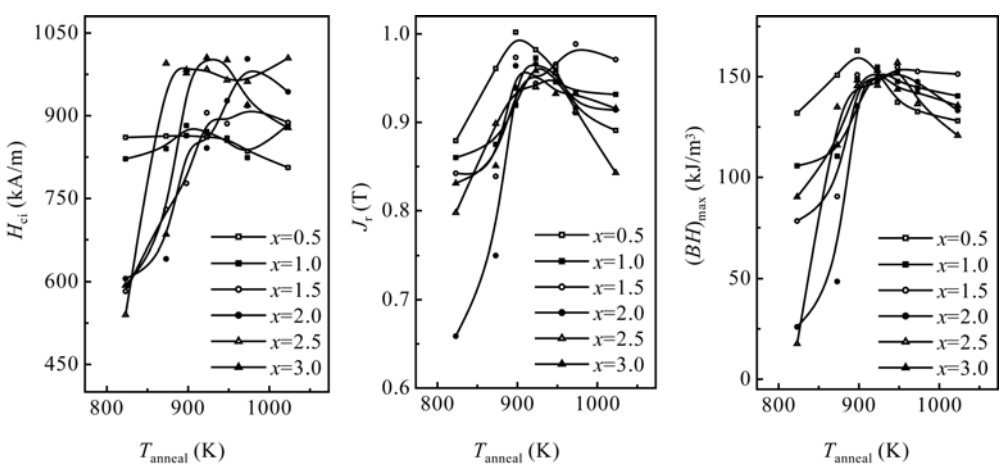

Figure 4 J_r, H_{ci} and $(BH)_{max}$ of $Nd_{12.3}Fe_{81.7-x}Zr_xB_{6.0}$ ribbons as a function of annealing temperature for 10 min.

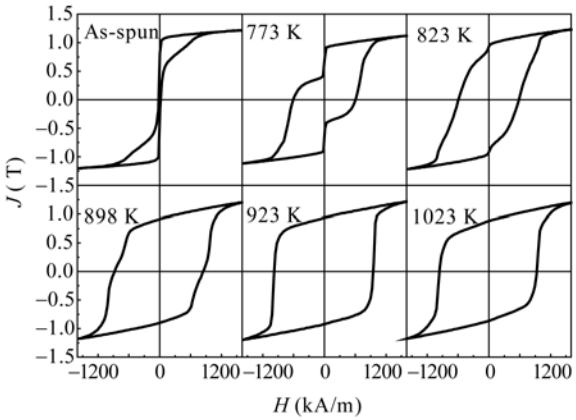

Figure 5 Hysteresis loops for the ribbons with $x = 3.0$ in as-cast and devitrification annealing states.

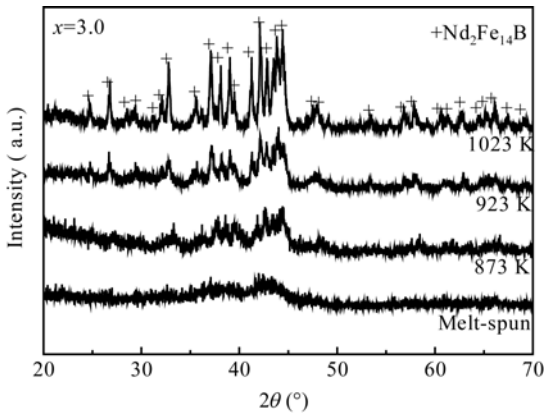

Figure 6 XRD patterns for the ribbons with $x = 3.0$ in melt-spun and devitritication annealing states.

magnetically soft behavior and a very low coercivity due to a large amount of residual amorphous phase. High coercivities are developed after crystallizing the melt-spun ribbons into a fine tetragonal $Nd_2Fe_{14}B$-type crystal structure. A smooth hysteresis loop with good squareness and decent magnetic properties have been obtained in the sample annealed at 923 K. Squareness of the demagnetization curves and the magnetic properties decrease with further increasing annealing temperature due to the presence of coarse grains as evidenced by a decrease in the half-width of the characterization peaks. It is worth remarking that a Zr-rich phase of Zr_3Fe reported by Betancourt[16] in $(NdPr)_8Fe_{86-x}Zr_xB_6$ ($x = 1-4$) ribbons is not identified in this investigation.

2.3 Influence of Zr content on magnetic properties and microstructure

Figure 7 summarizes J_r, H_{ci} and $(BH)_{max}$ of the optimum $Nd_{12.3}Fe_{81.7-x}Zr_xB_{6.0}$ ribbons as a function as Zr content, respectively. The intrinsic coercivitiy H_{ci} of the opti

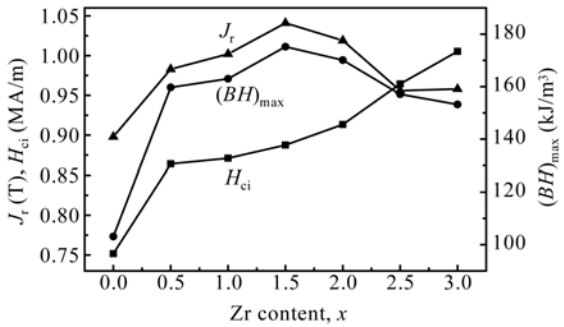

Figure 7 Variation of the optimal J_r , H_{ci} and $(BH)_{max}$ with Zr content.

mally processed $Nd_{12.3}Fe_{81.7-x}Zr_xB_{6.0}$ ribbons increases from 751.7 kA/m for $x = 0$ to 1005.3 kA/m for $x = 3.0$, which is in good agreement with most reports[17,18], but differs from the observations by Raviprasad[19] and Chen[20]. The remanence polarization J_r and maximum energy product $(BH)_{max}$ increase first with increase x until reaching the maximum values, then slightly decrease with further increasing of x. Optimum magnetic properties with J_r = 1.041 T, H_{ci} = 887.5 kA/m and $(BH)_{max}$ = 175.2 kJ/m^3 are achieved by annealing melt-spun the ribbons with $x = 1.5$ at 898 K for 10 min. XRD patterns of $Nd_{12.3}Fe_{81.7-x}Zr_xB_{6.0}$ ribbons annealed at 923 K for 10 min are shown in Figure 8. It is found that all the major diffraction peaks can be indexed to the 2∶14∶1 characteristic signals, revealing the single-phase materials. No additional peaks or phases with Zr addition are detected. The main appreciable change in the XRD patterns is the peak broadening with Zr addition, indicating reduction of grain sizes. All ribbons have a high saturation remanence ratio of 0.75 or so, suggesting the existence of the intergranular exchange-coupling effect in all samples, which is similar to the typical nanocomposite magnet.

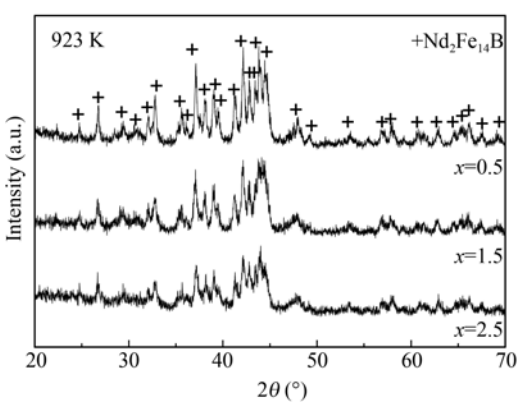

Figure 8 XRD patterns for $Nd_{12.3}Fe_{81.7-x}Zr_xB_{6.0}$ ribbons annealed at 923 K for 10 min.

Since magnetic properties change with Zr addition significantly, and there is strong relationship between microstructure and magnetic properties of nanocrystalline alloy, it is very necessary to understand the details of microstructure evolution to further understand the effect of Zr addition in the $Nd_{12.3}Fe_{81.7}B_6$ alloys. In order to understand the detailed microstructure evolution, three regions through the $Nd_{12.3}Fe_{81.7-x}Zr_xB_{6.0}$ ribbon thickness, i.e., near-free surface, inner part and near-wheel-contacted surface, were investigated in HRSEM observations. Figure 9 shows images of fracture surfaces through thickness of the ribbons. From Figures 9(a), (b) and (c), the microstructure from the free surface to the wheel-contacted surface through ribbon thickness appears to be a single-phase nanostructure. It is found that the average grain size differs from the roll contact side to the free side of the flakes. It is clear from Figures 9(d), (e) and (f) that microstructure is significantly refined by small amount of Zr addition. The average grain sizes reduce from 80 nm for $x = 0$ to 25 nm for $x = 3.0$. It can be concluded that appropriate Zr addition results in an increase in J_r because of the contribution of the stronger exchange coupling interactions.

3 Discussion

Analysis of $Nd_{12.3}Fe_{81.7-x}Zr_xB_{6.0}$ ribbons prepared at the wheel speed of 22 m/s shows that the samples with $x > 1.0$ contain a little amorphous phase. The magnetic properties of the samples with $x < 1.0$ are not high, although the samples consisted fully of crystalline phase. To obtain the best magnetic properties, it is necessary to anneal the samples. According to the results of Figures 3 and 4, the annealing temperature is slightly higher than the temperature at which 2∶14∶1 phase is formed. If the temperature is lower, the 2∶14∶1 phase is not fully formed, so that the magnetic properties are not good. For the condition that the temperature is too high, the grain of the 2∶14∶1 phase is coarse, and the magnetic properties are still not good. Because the crystallization temperature of the alloy with $x = 2.5$ is higher than those of the alloys with $x = 1.5$, it is expected that the annealing temperature of the alloy with $x = 2.5$ will be higher than those of the alloys with $x = 1.5$. The experimental results show that the annealing temperature for the alloy with $x = 2.5$ with the best magnetic properties is higher than those for the alloys with $x = 1.5$.

$Nd_{12.3}Fe_{81.7-x}Zr_xB_6$ alloys are composed of predominant $Nd_2Fe_{14}B$ phase. Remanence enhancement is observed in all alloys. The alloys have a high saturation remanence ratio, suggesting a possibility of the presence of the exchange-spring mechanism. Therefore, it can be concluded that exchange-coupling effect between grains should play an important role in the $Nd_{12.3}Fe_{81.7-x}Zr_xB_6$ alloys, which is similar to the typical nanocomposite magnet with low Nd content containing a larger volume fraction of the soft phase. Therefore, Zr atoms are thought to behave similarly in both the nanocomposite magnet with a lower Nd content and the nanocrystalline magnet with a high Nd content. Small amount of Zr addition significantly improves coercivity and remanence of the nanocrystalline magnets. Microstructural changes of the Zr-doped alloys may play a critical role in developing the high magnetic properties values. Zr has very low solubility in $Nd_2Fe_{14}B$ phases; therefore, Zr atoms are

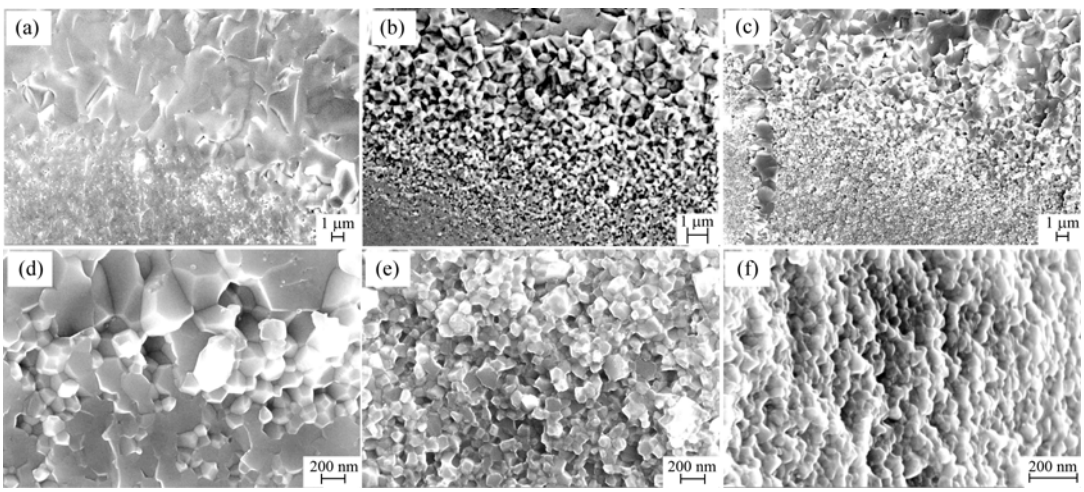

Figure 9 HRSEM images of $Nd_{12.3}Fe_{81.7-x}Zr_xB_{6.0}$ ribbons optimally processed. (a)(d) x=0; (b)(e) x=1.5; (c)(f) x=3.0.

expelled from $Nd_2Fe_{14}B$ phases during melt-spinning and annealing processes, resulting in the enrichment of Zr atoms at the grain boundary region and generation of Zr-rich phase along grain boundary, which inhibits the grain growth and finally refines the microstructure.

4 Conclusion

To sum up the above-mentioned results and analysis, the effects of adding Zr to $Nd_{12.3}Fe_{81.7}B_{6.0}$ permanent magnetic alloys are: (1) the tendency to form amorphous phase is enhanced; (2) the crystallizing temperature is increased; (3) the grain size of the $Nd_2Fe_{14}B$ phase is refined; (4) the coercivity and remanence are increased, so that high magnetic properties with $J_r = 1.041$ T, $H_{ci} = 887.5$ kA/m and $(BH)_{max} = 175.2$ kJ/m^3 are achieved for the ribbons with $x = 1.5$.

1 Liu Z W, Davies H A. The practical limits for enhancing magnetic property combinations for bulk nanocrystalline NdFeB alloys through Pr, Co and Dy substitutions. J Magn Magn Mater, 2007, 313(2): 337－341[doi]

2 Gholamipour R, Beitollahi A, Marghusian V K, et al. Cu effects on coercivity and micro-structural features in nanocrystalline Nd-Fe-Co-B annealed melt-spun ribbons. Physica B, 2007, 398(1): 51－54[doi]

3 Li X H, Gao Z S, Li W, et al. Study of the microstructure of α-Fe/$Nd_2Fe_{14}B$ nanocomposites prepared by electropulsing heating amorphous NdFeCoB. Mater Lett, 2005, 59(22): 2782－2785[doi]

4 Pampillo L G, Saccone F D, Sirkin H R. Structural and magnetic properties of nanocrystalline $Nd_{4.5}Fe_{72}Co_2Cr_3Al_1B_{17.5}$ ribbons. Physica B, 2007, 389(1): 172－175[doi]

5 Yang C J, Park E B, Hwang Y S, et al. The effect of Co on the enhanced magnetic properties of $Fe_3B/Nd_2Fe_{14}B$ magnets. J Magn Magn Mater, 2000, 212(1-2): 168－174[doi]

6 Yang C P, Jiang Z L, Chen X Y, et al. Microstructure and magnetic properties of two-phase nanocomposite $Nd_9Fe_{85.5}Nb_{1.0}B_{4.5-y}C_y$ (y = 0.5－4.5) magnets. J Alloy Compd, 2001, 316(1-2): 269－274[doi]

7 Harland C L, Davies H A. Magnetic properties of melt-spun Nd-rich NdFeB alloys with Dy and Ga substitutions. J Alloy Compd, 1998, 281(1): 37－40[doi]

8 Ahmad I, Davis H A, Buckley R A. The effect of Nd content on the structure and properties of melt spun Nd-rich NdFeB alloys. J Magn Magn Mater, 1996, 157-158(1): 31－32

9 Lewis L H, Collins S M, Kramer M J, et al. Solidification, quenching gas and magnetic properties in melt-spun $Nd_2Fe_{14}B$. IEEE T Magn, 2001, 37(4): 2486－2488[doi]

10 Zhang W Y, Chang H W, Chiu C H, et al. Beneficial effect of the substitution of Co for Fe on the magnetic properties of melt-spun $Pr_2Fe_{14}C/\alpha$-Fe-type nanocomposite magnets. J Alloy Compd, 2004, 379(1): 28－30

11 Wang C, Yan M, Zhang W Y. Significant changes in the microstructure, phase transformation and magnetic properties of $(Nd,Pr)_2Fe_{14}B/\alpha$-Fe magnets induced by Nb and Zr additions. Mater Sci Eng B, 2005, 123(1): 80－83[doi]

12 Ohkubo T, Miyoshi T, Hirosawa S, et al. Effects of C and Ti additions on the microstructures of $Nd_9Fe_{77}B_{14}$ nanocomposite magnets. Mater Sci Eng A, 2007, 449-451(12): 435－439[doi]

13 Tian Z J, Li S D, Peng K, et al. The microstructure and magnetic properties of NdFeB magnets directly solidified at a low cooling rate. Mater Sci Eng A. 2004, 380(12): 143－146[doi]

14 Bao X Q, Qiao Y, Gao X X, et al. Effect of annealing time on exchange coupling interactions and microstructure of nanocomposite $Pr_{7.5}Dy_1Fe_{71}Co_{15}Nb_1B_{4.5}$ ribbons. J Univ Scid Technol Beijing, 2007, 14(6): 547－551

15 Daniil M, Zhang Y, Okumura H, et al. Effect of grain growth inhibitors on the hysteresis properties of $Nd_{10}Fe_{82}C_6B_2$ melt-spun alloys. IEEE T Magn, 2002, 38(5): 2973－2975[doi]

16 Betancourta I, Davies H A. Influence of Zr and Nb dopant additions on the microstructure and magnetic properties of nanocomposite $RE_2(Fe,Co)_{14}B/\alpha$(Fe,Co) (RE=Nd-Pr) alloys. J Magn Magn Mater, 2003, 261(3): 328－336[doi]

17 Wu Y Q, Ping D H, Xiong X Y, et al. Magnetic properties and microstructures of α-Fe/$Nd_2Fe_{14}B$ nanocomposite microalloyed with Zr. J Appl Phys, 2002, 91(10): 8174－8176[doi]

18 Feng S S, Ni J S, Wang Z Y, et al. Influence of zirconium addition on the microstructure and magnetic properties of nanocomposite $Nd_{10.1}Fe_{78.2-x}Co_5Zr_xB_{6.7}$ permanent magnets. Rare Metals, 2007, 26(3): 218－221[doi]

19 Raviprasad K, Ravishankar N, Chattopadhyay K, et al. Magnetic hardening mechanism in nanocrystalline $Nd_2Fe_{14}B$ with 0.1 at% addition of Cr, Cu, or Zr. J Appl Phys,1998, 83(2): 916－920[doi]

20 Chen Z, Smith B R, Brown D N, et al. Effect of Zr substitution for rare earth on microstructure and magnetic properties of melt-spun $(Nd_{0.75}Pr_{0.25})_{12.5-x}Zr_xFe_{82}B_{5.5}$ (x = 0－3.0) ribbons. J Appl Phys, 2002, 91(10): 8168－8170[doi]